

PAPER • OPEN ACCESS

A four-terminal-pair Josephson impedance bridge combined with a graphene-quantized Hall resistance












To cite this article: S Bauer *et al* 2021 *Meas. Sci. Technol.* **32** 065007

View the [article online](#) for updates and enhancements.

You may also like

- [The quantized Hall resistance: towards a primary standard of impedance](#)
F Overney, B Jeanneret, B Jeckelmann et al.
- [The quantum Hall impedance standard](#)
J Schurr, J Kuera, K Pierz et al.
- [Realizing the farad from two ac quantum Hall resistances](#)
J Schurr, V Bürkel and B P Kibble

A four-terminal-pair Josephson impedance bridge combined with a graphene-quantized Hall resistance

S Bauer¹ , R Behr¹ , R E Elmquist² , M Götz¹ , J Herick¹ , O Kieler¹ , M Kruskopf^{1,2} , J Lee¹ , L Palafox¹ , Y Pimsut^{1,3}  and J Schurr¹ 

¹ Physikalisch-Technische Bundesanstalt, Bundesallee 100, 38116 Braunschweig, Germany

² National Institute of Standards and Technology, 100 Bureau Drive, Stop 8171, Gaithersburg, MD 20899, United States of America

³ National Institute of Metrology Thailand, 3/4-5 Moo 3, Klong 5, Klong Luang, Pathumthani 12120, Thailand

E-mail: stephan.bauer@ptb.de

Received 7 October 2020, revised 3 November 2020

Accepted for publication 2 December 2020

Published 31 March 2021



CrossMark

Abstract

This paper introduces a four-terminal-pair impedance bridge based on pulse-driven Josephson junctions arrays which is designed to link any kind of impedance to the quantized Hall resistance. The unique features of the quantized Hall resistance in a multiple series connection allows to dispense a combining network and leads to a compact and simple design of the whole setup. Moreover, the low noise of a quantized Hall resistance reduces the measurement time compared to resistance standards at room temperature which is essential for the characterization of quantum Hall devices in the AC regime. A first measurement campaign confirmed the expected low noise of $1.82 \text{ nV}/\sqrt{\text{Hz}}$ for a link to a 10 nF capacitance standard. The repeatability of the bridge was found to be few parts in 10^8 . Capacitance and resistance standards were measured at 1233.15 Hz against graphene based quantum Hall resistance devices.

Keywords: impedance measurement, quantized Hall resistor, coaxial impedance bridge, graphene, Josephson arbitrary waveform synthesizer

(Some figures may appear in colour only in the online journal)

1. Introduction

Measurements of impedances play a major role in realizing and disseminating the electrical units and also for many fields in our daily life, which has encouraged development of a large variety of impedance bridges [1].

The well-known quantized Hall resistance (QHR) is a very good example for the use of quantum effects in metrology.

The QHR is the state-of-the-art standard for the unit ohm in the DC regime in the new SI [2–4]. Different approaches are used for realization of the electrical units, especially the unit farad. One possibility is to start with a calculable Thompson Lampard capacitor [5]. This method results in a rather short calibration chain if the targeted values are the commonly used 10 pF and 100 pF . Another possibility is to make use of the quantized Hall resistance. This solution splits up into two different routes. The first one starts from the DC QHR and uses resistors with well-known AC–DC transfer difference [6]. The second possibility is to use the QHR directly operated at AC which allows not only to omit the artefact for the AC–DC transfer, but has further metrological advantages [7]. In the past, this route could only be



Original Content from this work may be used under the terms of the [Creative Commons Attribution 4.0 licence](https://creativecommons.org/licenses/by/4.0/). Any further distribution of this work must maintain attribution to the author(s) and the title of the work, journal citation and DOI.

realized by precise and complex impedance bridges based on inductive voltage dividers (IVD). To get the 90° phase angle needed for a comparison of a resistance and a capacitance, this bridge employs a double quadrature bridge with two QHR and two 10 nF capacitance standards. Because of the combination of two bridges, these devices are often called double quadrature bridges. By this method the calibration chain for capacitance is simplified and the measurement uncertainties are reduced compared to the chain starting with the DC QHR [7].

Using graphene based QHR devices will allow for relaxed experimental conditions as the operating temperature can be raised to that of liquid helium (^4He , 4.2 K). Also GaAs QHR devices can be operated at metrological precision [8] but the needed magnetic field is typically in the range above 6 T and the $i = 2$ plateau is smaller at this higher temperatures. The magnetic field can be reduced to the range of about 5 T using graphene based devices. Combining the higher temperature and the lower magnetic field allows to operate the graphene QHR in a compact closed cycle cryostat. This will reduce the costs and complexity of such systems and hence increase the appeal for smaller National Metrology Institutes, calibration laboratories and in future maybe also for industry [9–12].

The need for two QHR devices in a double quadrature bridge can be avoided by using a digital impedance bridge which is able to generate arbitrary and precise phase angles. An impedance bridge using two pulse-driven Josephson junction arrays (also called Josephson Arbitrary Waveform Synthesizer) is a special type of such a digital impedance bridge. The outstanding ability of JAWS to provide quantum-based AC signals with high accuracy and extremely low harmonic content [13] can efficiently be used for impedance metrology [14–16]. Using two independent JAWS systems allows to provide arbitrary voltage ratios with an arbitrary phase angle. Moreover, the possibility of generating arbitrary signals can also be used to investigate properties of the associated bridge setup e.g. generating a signal with defined harmonic content to investigate the response of the setup. The combination of Josephson voltage standards and a quantum Hall device provides perfect conditions for impedance metrology [15]. The possibility to generate arbitrary voltage ratios and phase angles also allows to compare e.g. 1 nF capacitance standards directly with the QHR. This reduces the calibration chain to the commonly used 10 pF capacitance standards by one step as presented in [16].

We will present the extension of PTBs two-terminal-pair impedance bridge to a four-terminal-pair definition as well as the results of a first measurement campaign. The paper is structured in the following way: First the experimental setup with all needed components will be introduced in section 2. Section 3 presents measurement results. Finally, section 4 will summarize the paper and will present an outlook for future work on this impedance bridge.

2. Experimental setup

The experimental setup was introduced in [17] and can be divided into three parts. The first one describes the pulse-driven Josephson system which provides the two potential definitions within the impedance bridge. The second part introduces the quantized Hall resistance setup. Finally the 4-TP bridge is explained including injection and detection transformer as well as sources and detectors.

2.1. Pulse-driven Josephson system

For the measurements reported here, two pulse-driven Josephson junction arrays were installed into a liquid helium Dewar. Each array can provide AC signals with amplitudes of over 100 mV using the AC coupling technique with compensation currents [18]. The rf pulse bias is realized by a pulse pattern generator (PPG; BPG 2x30G-TERx4, Sympuls⁴) with a clock speed of approximately 14 GHz and two independent memories. With this PPG, the output signal generated by one memory can be shifted in steps of one bit relative to the other memory. This results in a resolution of about 71 ps at 14 GHz clock frequency. The phase angle between the two signals can be fine tuned using an analog delay with 200 fs resolution, which is a perfect condition for the phase adjustment in impedance measurements. The Josephson arrays are mounted in a special chip carrier with two separated capsules to provide individual screens for each array (see figure 1) [19]. With this screening the crosstalk between both signals was below our detection limit of approximately -180 dB for frequencies less than 10 kHz and -146 dB at 100 kHz. This was measured at the output of one JAWS that was switched off with a lock-in amplifier while the other array was operated at the nominal amplitude of 100 mV.

The spurious free dynamic range (SFDR), measured with a NI PXI-5922 is at least 115 dBc at 1233.15 Hz as shown in figure 2. This high spectral purity avoids any mixing of higher harmonics into the measurement frequency due to non-linear response of e.g. pre-amplifiers.

The range of bias parameters over which the SFDR is not affected, is often called operating margins, flat spot or quantum-locking range (QLR). In order to determine this QLR, both Josephson systems were checked by two types of measurements. The first possibility is to add a low frequency current to the array. The maximum additional current which does not affect the SFDR is a measure of the QLR of the system. For the two arrays used in this measurements, the maximum additional low frequency currents are 1.13 mA for array 1 and 0.85 mA for array 2.

The second way is to check the range of bias parameter in which the SFDR of the output signal is not changed. This was carried out before the measurement campaign and each

⁴ Identification of commercial equipment does not imply an endorsement by PTB or that it is the best available for the purpose.

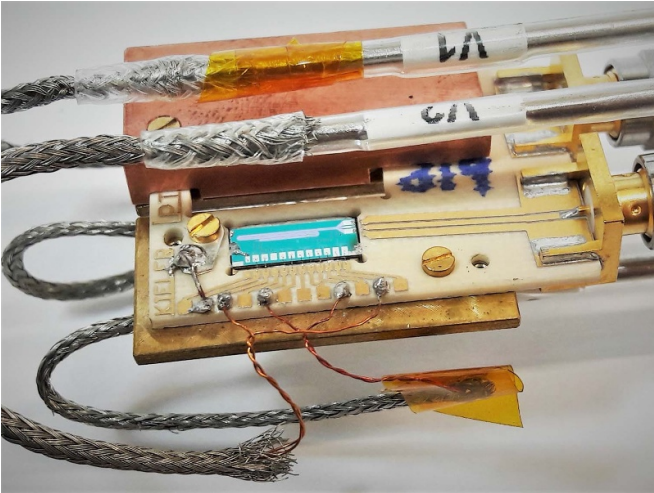


Figure 1. Picture of the chip carrier for the two Josephson junction arrays. The top cover of the first array is removed in this photo.

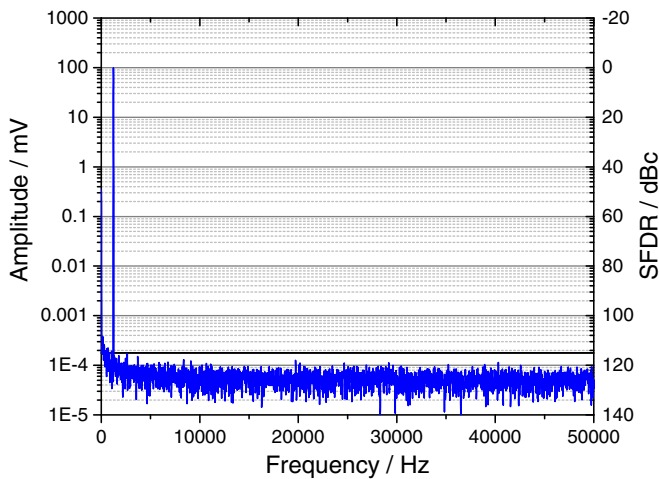


Figure 2. Measured spectrum of the output signal of array 1 at 1233.15 Hz. The SFDR is less than 115 dBc, as indicated by the black line.

bias parameter was set to the center value of the range found. For this purpose, the 4-TP impedance bridge offers a highly sensitive detection of changes in the output voltage. When the impedance bridge is balanced (see section 2.3.1) any change in the output voltage due to a change of bias parameters of one system will directly change the detector reading. This measurement turned out to be more sensitive than the SFDR measurements, which remained unchanged even though the detector had shown changes. Detailed measurements were not carried out during these proof of principle measurements since the measurement time was limited and some effects will cancel out as long as they are stable over the measurement time as reported in [16]. We will perform a detail study of this dependency as part of the process to determine the complete uncertainty budget for this bridge.

An inductive voltage drop will occur due to the bias current at the signal frequency and the inductance of the coplanar wave guide in which the Josephson junctions are arranged. The

inductance of the Josephson junction arrays was measured at 100 kHz to be 15 nH for array 1 and 16 nH for array 2. The estimated uncertainty for the inductance measurement is 5%. This voltage is shifted by approximately 90° and hence mainly affects the imaginary part of the measurement. Moreover, as long as the inductive voltage drop does not change, the influence on the result cancels out when the impedances are interchanged and remeasured as described later in section 2.3. Small changes in the output voltage are needed to balance the bridge or to determine the sensitivity of the setup, but the inductive voltage drop will not change since the compensation current remains constant. The phase of the compensation current is set such that the in-phase component of the main detector remains constant while changing the compensation current [17].

2.2. Quantized Hall resistance setup

The QHR sample was mounted in a EUROMET coaxial sample holder developed by METAS [21] and operated inside a cryomagnet system at 4.2 K. The maximum field is ± 12 T. Based on the geometry of the contacts of our QHR device, we set the current of the magnet so that the magnetic field vector points perpendicular out of the plane of the two-dimensional electron gas when viewed as in figure 3. For the reverse orientation of the magnetic field, the quantum Hall voltage is measured diagonally instead of orthogonally, which might be less favored because of a superimposed longitudinal voltage. The setup is equipped with coaxial cables and hence allows to perform DC and AC measurements.

All measurements presented in this work were carried out with a graphene QHR sample provided by NIST [22]. The sample is doped by chromium tricarbonyl for charge carrier density control [23]. By gently heating the sample in an inert gas atmosphere at 150°C, the carrier density was adjusted to a low n-type level between $1.0 \times 10^{11} \text{ cm}^{-2}$ to $3.1 \times 10^{11} \text{ cm}^{-2}$ during different cool downs. The electric contacts of the device use superconducting NbTiN as well as a branched design to minimize dissipation in the triple-series connection [24, 25].

2.3. Impedance bridge setup

The impedance bridge is an extension of the existing two-terminal-pair setup [15]. A schematic diagram is shown in figure 3 and represents a classical four-terminal-pair (4-TP) bridge. It consists of a potential arm and a current arm for each of the two impedances. Within this bridge the defining conditions for a 4-TP measurement must be fulfilled. Hence the currents inside the potential arms must be zero. This is achieved by adjusting the current injection (S_1 and S_2) such that the measured currents in the potential arms at the detection transformers (D_1 and D_2) become zero. For this specific setup the detection transformers are read out by a 2 channel lock-in amplifier (HF2LI, Zurich Instruments) and the outputs of this device are used for the current injection. The 10 k Ω resistors in the current arms reduces the influence of the stability and

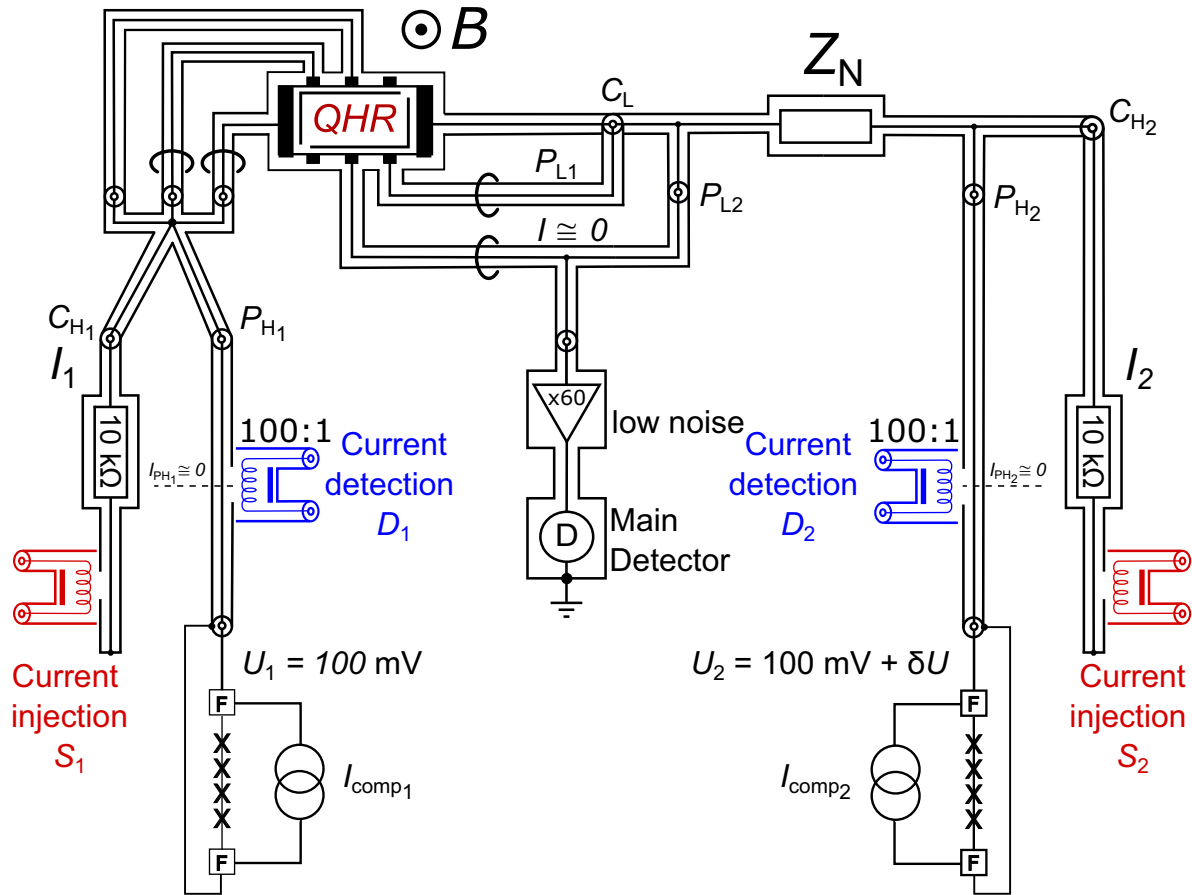


Figure 3. Schematic diagram of the impedance bridge setup. The QHR device is connected in a triple-series connection [20] and located inside a cryomagnet system at 4.2 K. The two Josephson junction arrays (represented as XXXX) are located inside a liquid Helium Dewar and providing the potential definition for both impedances. The current inside the potential lines is measured over 100:1 detection transformer (D_1 and D_2). The measurement current is provided by two function generators (S_1 and S_2) over an injection transformer with a 10 k Ω resistor in series. In each mesh an active equalizer (represented as black circles around the coaxial cables) is installed to ensure the coaxiality of the bridge. The measured signal is amplified by a low noise pre-amplifier by a factor of 60 © 2020 IEEE. Reprinted, with permission, from [17].

noise of the function generators by the ratio of the output resistance of the JAWS system to the 10 k Ω resistors as described in detail in [14]. Typically the output resistance of the JAWS is dominated by the connecting cable and is on the order of 1 Ω .

The potential definitions are provided by the two JAWS systems where U_1 is fixed to 100 mV and the amplitude and the phase angle of U_2 is adjusted to minimize the reading of the main detector. We used a low noise pre-amplifier [26] with a gain of approx. 60 to reduce the influence of the input noise of the commercial lock-in amplifier (MFLI, Zurich Instruments) used. The amplification factor is sufficiently stable over the measurement and the absolute value did not have to be known in advance, since it is included in the sensitivity measurement as explained later.

The 10 MHz clock of the PPG and the function generators are linked to the optical 10 MHz reference signal provided by the time and frequency division of PTB. The PPG not only provides the pulse streams for the JAWS but also the reference signal for the lock-in amplifiers, which therefore measuring at exactly the same frequency as the output signal of the Josephson voltage standards.

Compared to impedance bridges using room-temperature resistance standards as reference, the combination of an impedance bridge and a quantized Hall resistance offers a much lower noise level due to the temperature of 4.2 K of the QHR. The expected noise can be calculated by:

$$e_N = \sqrt{e_N^2(\text{PA}) + e_N^2(\text{QHR}) + e_N^2(Z)}, \quad (1)$$

where $e_N(\text{PA})$ is the equivalent input noise of the pre-amplifier, $e_N(\text{QHR})$ the noise of the quantized Hall resistance and $e_N(Z)$ the noise of the impedance under test. For a capacitance standard the equivalent noise can be assumed as zero in the first order. The gain of the preamplifier reduces the contribution from the lock-in amplifier to the overall noise to 0.001 nV/ $\sqrt{\text{Hz}}$ and is therefore not included in equation (1).

The measurement shows a noise of (1.8 ± 0.2) nV/ $\sqrt{\text{Hz}}$ for a comparison of a 10 nF capacitance standard and the QHR. The calculated noise for this configuration is 1.82 nV ($\sqrt{\text{Hz}}$) $^{-1}$. For a ratio measurement using a 12.9 k Ω

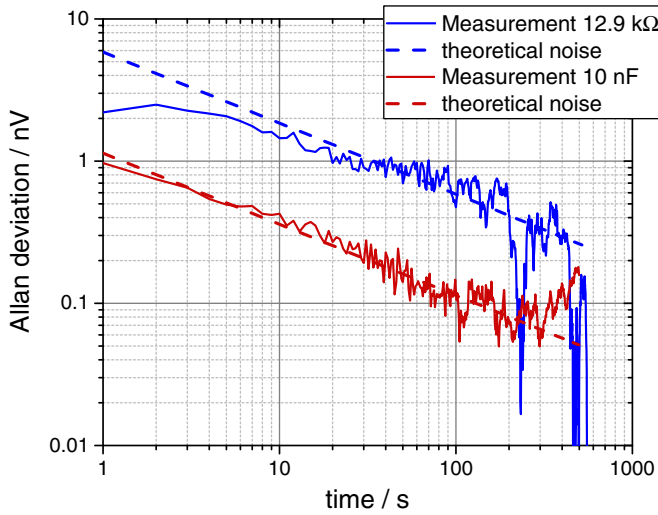


Figure 4. Plot of the Allan deviation for the measurement of a 10 nF capacitance standard and a 12.9 k Ω each against the QHR at 4.2 K. The Allan deviation was calculated from the pre-amplifier input signal taking the measurement bandwidth of lock-in amplifier into account. This was 0.156 Hz for the QHR to the 12.9 k Ω resistance measurement and 0.391 Hz for the measurement of the 10 nF capacitance standards to the QHR.

resistance standard temperature stabilized at 30 °C and the QHR, the setup showed $(14.9 \pm 0.4) \text{ nV} (\sqrt{\text{Hz}})^{-1}$ and the calculated noise is $14.8 \text{ nV} (\sqrt{\text{Hz}})^{-1}$. This clearly shows that there is no significant additional noise generated by the setup (e.g. no electrical interference from function generators or other components). This can also be seen from the Allan deviations as shown in figure 4.

2.3.1. Bridge balance procedure. During the first measurements with this system the bridge was balanced manually. After the two Josephson voltages were applied, the output signals of the function generators (S_1 and S_2) were set such that the readings of the current detectors (D_1 and D_2) were minimized. In the next step the phase between both JAWS systems was adjusted to minimize the reading of the main detector. Then, the voltage U_1 was changed temporarily by 10^{-4} V/V to measure the change in detector reading and to properly adjust the reference phase of the lock-in amplifier. From the change in detector voltage U_D and the known change of U_1 , the sensitivity coefficient S can be determined to quantify how much the detector reading will change if the ratio of the applied voltages or the impedance ratio changes by a certain amount. With this sensitivity coefficient and the previous reading of the main detector, a new voltage U_2 was calculated and applied. This procedure was repeated until the main detector reading was typically below 100 nV (250 nV at maximum). The detector signal U_D was used together with the measured sensitivity S and the voltage ratio applied to calculate the impedance ratio using equation (2). The remaining signal at the input of the detector corresponds typically to a correction of some parts in 10^8 . The detector signal and the sensitivity coefficient must be known to about 1% to achieve an uncertainty of the balance itself of 1 part in 10^9 .

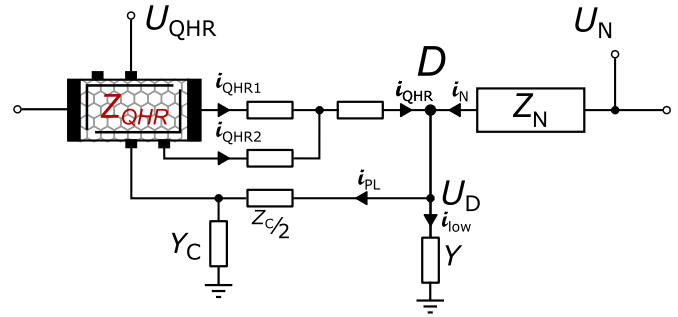


Figure 5. Low part connection of the impedance bridge. The two current cables of the triple-series connection are connected to the current low connection of the impedance (Z_N). The potential cable of the QHR is connected to the potential low of Z_N . The admittance Y_C and impedance Z_C belong to the potential low cable. The sum of the detector admittance and of all connecting cables of the low part of the bridge is represented as Y . The outer conductor is omitted for clarity.

After this *forward* measurement the impedances are interchanged by changing the potential high and current high connections of the bridge from one impedance to the other. Now the bridge is rebalanced as described above and a *reversed* measurement is carried out.

Due to the properties of a QHR in a triple-series connection [20], the current in the potential defining terminal is so small that the direct contribution of the lead and contact resistances becomes negligible and the effect of the lead capacitive current is considered as a conventional and very small cable correction. This offers the opportunity to omit a *Kelvin* combining network at the low side of the bridge which is usually needed in 4-TP impedance bridges. The currents of the inner conductors of the three cables at the low side of the QHR were measured to ensure that the current in the potential low connection is sufficiently small. The measurement was carried out using a 100:1 current detection transformer which detection voltage was read by a lock-in amplifier. The remaining current inside the low potential lead is 1.4×10^4 times smaller than the measurement current and hence influences the measurement only by about 5 parts in 10^9 , for a sum of cable and contact resistance of about 1 Ω . Nevertheless, this influence will not limit our results in this measurement campaign.

The model equation of the impedance bridge can be derived by Kirchhoff's law. The impedance ratio can be calculated by summing all currents in node D of figure 5:

$$\frac{Z_N}{Z_{\text{QHR}}} = -\frac{U_N}{U_{\text{QHR}}} + \frac{U_D}{U_{\text{QHR}}} \cdot S, \quad (2)$$

$$S = G^{-1} \cdot \left(1 + Z_N(Y + Y_C) + \frac{Z_N}{Z_{\text{QHR}}} \right), \quad (3)$$

where Z_N is the impedance to be compared with the impedance of the QHR (Z_{QHR}) and S the sensitivity coefficient. Y is the sum of all admittances of the connecting cables at the low side and that of the pre-amplifier. U_N and U_{QHR} are the voltages applied to the impedances. U_D the voltage measured

at the input of the detector and G the amplification factor of the pre-amplifier. For almost all practical setups the contribution of $Z_c/2$ will not influence the sensitivity coefficient to a level higher than 10^{-3} for frequencies up to 100 kHz. Therefore, this term is assumed as zero in equation (3).

Equation (3) can be used to calculate the sensitivity coefficient of the impedance bridge. For this purpose the capacitance of the connecting cables at the low side was measured using a commercial LCR meter. For a comparison of a 10 nF capacitance standard and the QHR at 1233.15 Hz a coefficient of 0.0281 is measured and is in sufficient agreement with the one of 0.0278 predicted by equation (3). In the case of a ratio measurement of QHR and a 12.9 k Ω resistance standard the measured value is 0.034 and agrees well with the calculated value of 0.0355. Combining the sensitivity coefficient with the noise level of the bridge gives the achievable Type A uncertainty of the setup. This is at a measurement time of 100 s, 1.9 nF/F for the measurement with the QHR and a 10 nF capacitance standard and 12 n Ω/Ω for the ratio measurement with a 12.9 k Ω resistance standard.

When the bridge is perfectly balanced ($U_D = 0$) equation (2) simplifies to the well-known relation, where the ratio of the impedances is given by the ratio of the voltages applied:

$$\frac{Z_N}{Z_{QHR}} = -\frac{U_N}{U_{QHR}}. \quad (4)$$

With the set of forward and reversed measurements as described above, effects like cable loading or small voltage bias cancel out as long as they are stable over time. The impedance ratio can be calculated as described in detail in the appendix of [16]:

$$\frac{Z_N}{Z_{QHR}} = \sqrt{\left(\frac{Z_N}{Z_{QHR}}\right)_F \left(\frac{Z_N}{Z_{QHR}}\right)_R} \quad (5)$$

where F and R denotes the ratio obtained by the *forward* and the *reverse* measurement respectively. The ratios themselves are calculated according to equation (2).

3. First measurement results

All measurements were carried out in the DC QHR laboratory of PTB. The JAWS system was moved to the QHR lab and operated in a liquid helium Dewar. In this proof of principle measurement, we focused on the in-phase component or real part of the impedance ratio. The imaginary part of the impedance ratio needs much more detailed and careful investigations due to the influence of an inductive voltage drop of the JAWS. This is out of the scope of this paper.

3.1. Linking capacitance standards to the QHR

Within this measurement campaign two 10 nF capacitance standards were measured against the QHR. Beside testing the new bridge setup, these measurements were also used to test new graphene based QHR devices [25]. The calibrated 10 nF

capacitance standards allowed us to investigate the properties of the graphene QHR, e.g. at different magnetic fields. The capacitance standards were measured against a 1 nF capacitance standard linked to a GaAs QHR. This was carried out four times over a period of 112 days using PTBs classical 10:1 ratio bridge based on inductive voltage dividers (IVD) [7]. Both standards show a drift of less than $\pm 2 \times 10^{-9}$ per day.

The first measurements were carried out to determine the deviation of the quantized Hall resistance at AC from its quantized DC value. This was performed in a quadrature measurement at 1233.15 Hz. To find the best operating point for the QHR the impedance bridge was balanced with the QHR operated at -12 T and 4.2 K. Then the magnetic field was slowly changed to -2.5 T at a constant rate of 0.15 T min $^{-1}$ without re-balancing the bridge. From the lock-in reading, the change in resistance of the QHR can be calculated since the value of the capacitor will stay unchanged during this measurement. Compared to measurements in a ratio bridge against a room-temperature resistance standard, this method profits from much lower noise and hence, needs only half of the measurement time (typically 1 h compared to 2 h). Even if the absolute accuracy of the new 4-TP bridge is not yet evaluated and these measurements are carried out without interchanging the impedances, they provide an important insight to the QHR sample. By this procedure the device can be investigated and shows in the ideal case a region where the resistance is independent of the magnetic field. For example, the influence of different geometries of the devices can be measured and compared.

The results for four different charge carrier densities, set as describes in section 2.2, can be seen in figure 6. The measurements show that for all except the highest carrier density, the deviation from the quantized resistance value is within $\pm 5 \times 10^{-8}$ for magnetic fields between -10 T and -12 T taking the calculated cable correction of the setup into account.

The value of the graphene QHR was measured multiple times against two 10 nF capacitance standards at 1233.15 Hz and a fixed magnetic field of -12 T. The results for different charge carrier densities are shown in figure 7. Also these results are all within $\pm 5 \times 10^{-8}$ of the DC quantum Hall value. The scattering of the data points and also the change of the mean value with respect to the charge carrier density can be related to properties of the sample that change with thermal cycling or to the reproducibility of the bridge. The latter will be investigated in the next evaluation of the bridge. This type of measurement will be used with a new cryo magnet at 4.2 K to investigate new graphene QHR samples and to determine the deviation of the quantized Hall resistance at AC from its DC value at different frequencies once the full evaluation of the bridge is performed.

3.2. Linking resistance standards to the QHR

The bridge was also used to compare a 12.9 k Ω resistance standard with the graphene QHR in a ratio measurement.

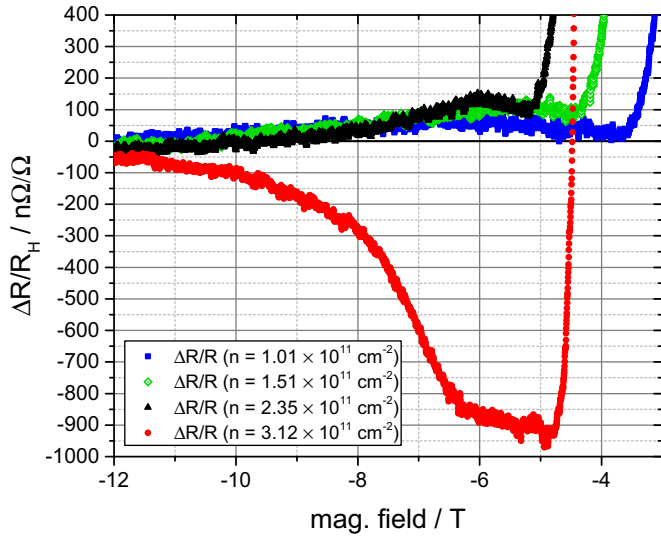


Figure 6. Magnetic field dependence of a quantized Hall resistor. The impedance bridge was balanced at -12 T and then the field was swept with a rate of 0.15 T min^{-1} . The lock-in reading was used to measure the change in the resistance value of the QHR device. The plot shows the relative difference between the measured resistance and the nominal value of the quantized Hall resistance R_H at the $i = 2$ plateau.

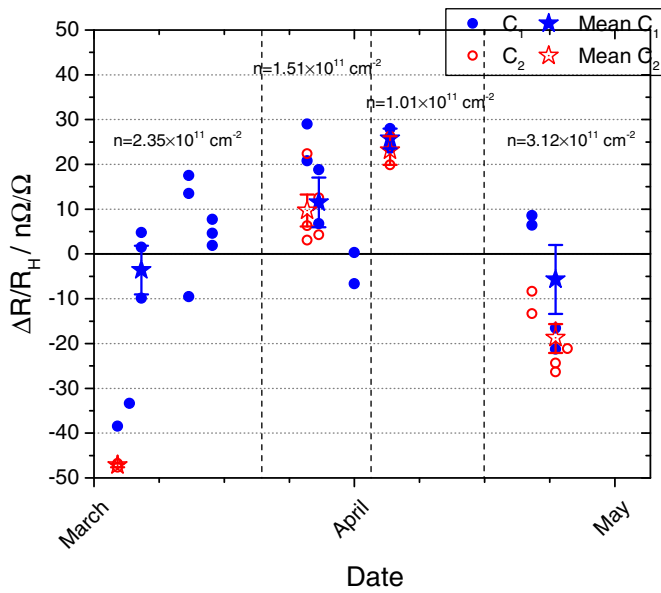


Figure 7. Overview of the measurements linking the QHR and two 10 nF capacitance standards. The measurements were carried out with four different charge carrier densities of the QHR. The round symbols denote one single set of forward and reversed measurement. The mean value over all measurements at one carrier density is shown as star.

Since the deviation of the QHR device from its DC value was already measured by the previous described quadrature measurements, we can use these results to determine the value of the resistance standard. In this case the graphene QHR acts as a transfer standard. All measurements

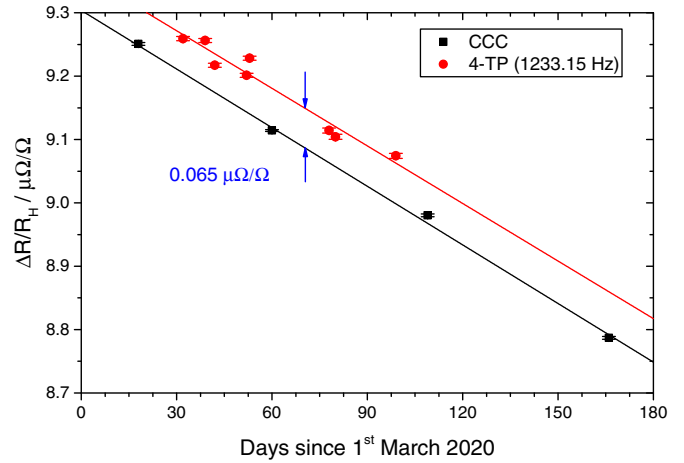


Figure 8. Plot of the stability of a $12.9\text{ k}\Omega$ resistance standard measured against a 10 nF capacitance standard using the QHR as transfer standard. The drift over time was also measured with a 14bit CCC at DC. The measured frequency dependence of the $12.9\text{ k}\Omega$ resistance standard was corrected. Cable corrections were not accounted for as they are almost the same in both measurements at AC and hence cancel out for the time dependence of the standard. The error bars corresponds to the Type A uncertainties for the measurements with the impedance bridge and the combined uncertainty ($k = 1$) for the CCC measurements.

were carried out at 1233.15 Hz and at the maximum field of -12 T . Moreover, the resistance standard was measured four times at DC with a 14bit cryogenic current comparator (CCC) against the national resistance standard of PTB. Figure 8 shows the stability of the resistance standard measured against the 10 nF capacitance standard using the graphene QHR as a transfer standard at 1233.15 Hz . The daily drift determined for both methods by a linear fit is in perfect agreement:

$$\begin{aligned} &(-3.03 \pm 0.23)\text{ n}\Omega/\Omega \text{ (4-TP)} \\ &(-3.08 \pm 0.10)\text{ n}\Omega/\Omega \text{ (CCC)}. \end{aligned}$$

The frequency dependence of the resistance standard was measured with an IVB ratio bridge against a reference resistor. This was done in a frequency range between 1 and 5 kHz . Even though the frequency dependence of the resistance standard was taken into account, the difference between the values measured with the 4-TP bridge deviates $65\text{ n}\Omega/\Omega$ from those measured with the CCC. The reason for this can e.g. be caused by a non-linear frequency dependence at lower frequencies. Further measurements are needed to resolve the origin of this deviation. Nevertheless, the excellent agreement for the daily drift of the resistance standard between both systems shows that the 4-TP JAWS impedance bridge already has a high flexibility and reproducibility.

4. Conclusion and outlook

The setup and measurements presented here prove the principle that the combination of a quantized Hall resistance

with a 4-TP JAWS impedance bridge leads to a compact setup that works well without a combining network. Also the noise level of $(1.8 \pm 0.2) \text{ nV} (\sqrt{\text{Hz}})^{-1}$ of the setup was as low as predicted by theory. The QHR device showed a deviation from the quantized value of $\pm 5 \times 10^{-8}$ at 1233.15 Hz in a comparison with 10 nF capacitance standards calibrated via our conventional GaAs based QHR and IVD bridges [7]. Our first AC measurements with graphene based quantized Hall resistances at 4 K show very promising results for the characterization with capacitance and resistance standards. Using a quadrature measurement of the QHR against a capacitance standards allows us to carry out magnetic field sweeps with lower noise and even reduces the measurement time compared to ratio bridges using room-temperature resistance standards. This will be used to investigate upcoming graphene QHR samples and to give important feedback to the manufacturing process.

Within ratio measurements, the time dependent drift of a 12.9 k Ω resistance standard was determined in a substitutional measurement and agreed within the fit uncertainty of 0.23 n Ω / Ω with the measurements of a 14bit CCC. This gives a first impression of the reproducibility of the setup. Still the deviation between data points is higher than the Type A uncertainty which may be caused by a non-optimal manual balance of the bridge, problems with the bridge setup itself or unaccounted cable effects within the cryostat due to different helium levels.

In the next step, we will use a new cryomagnet system which is dedicated for AC measurements with graphene QHR samples. With this system we will evaluate and optimize the JAWS 4-TP bridge and new graphene QHR samples. A full evaluation of this bridge will be performed to set up an uncertainty budget for multiple frequencies.

Acknowledgments

The authors would like to thank Marco Kraus for fruitful discussion and Niklas Abraham, Judith Felgner, Susanne Gruber, Gerhard Muchow, Eckart Pesel, Kathrin Störr, Thomas Weimann for technical assistance. This work was supported in part by the Joint Research Project GIQS (18SIB07). This project received funding from the European Metrology Programme for Innovation and Research (EMPIR) co-financed by the participating states and from the European Unions' Horizon 2020 Research and Innovation Programme. The work of Y. Pimsut was supported by the Braunschweig International Graduate School of Metrology (B-IGSM).

ORCID iDs

S Bauer  <https://orcid.org/0000-0001-6242-2223>
 R Behr  <https://orcid.org/0000-0002-5480-443X>
 R E Elmquist  <https://orcid.org/0000-0001-9041-7966>
 M Götz  <https://orcid.org/0000-0001-8464-0651>
 J Herick  <https://orcid.org/0000-0001-9441-7699>
 O Kieler  <https://orcid.org/0000-0001-5193-8910>

M Kruskopf  <https://orcid.org/0000-0003-2846-3157>
 J Lee  <https://orcid.org/0000-0002-7382-8584>
 L Palafox  <https://orcid.org/0000-0001-7663-856X>
 Y Pimsut  <https://orcid.org/0000-0001-9210-6512>
 J Schurr  <https://orcid.org/0000-0001-7985-5770>

References

- [1] Overney F and Jeanneret B 2018 Impedance bridges: from Wheatstone to Josephson *Metrologia* **55** S119–S134
- [2] Jeckelmann B and Jeanneret B 2001 The quantum hall effect as an electrical resistance standard *Rep. Prog. Phys.* **64** 1603–55
- [3] Schurr J, Ahlers F and Kibble B P 2012 The ac quantum Hall resistance as an electrical impedance standard and its role in the SI *Meas. Sci. Technol.* **23** 124009
- [4] Rigosi A F and Elmquist R E 2019 The quantum hall effect in the era of the new SI *Semicond. Sci. Technol.* **34** 093004
- [5] Thompson A and Lampard D 1956 A new theorem in electrostatics and its application to calculable standards of capacitance *Nature* **177** 888–888
- [6] Gibbings D L H 1963 A design for resistors of calculable a.c./d.c. resistance ratio *Proc. Inst. Electr. Eng.* **110** 335–47
- [7] Schurr J, Bürkel V and Kibble B P 2009 Realizing the Farad from two ac quantum Hall resistances *Metrologia* **46** 619
- [8] Kucera J, Svoboda P and Pierz K 2019 AC and DC quantum hall measurements in GaAs-based devices at temperatures up to 4.2 K *IEEE Trans. Instrum. Meas.* **68** 2106–12
- [9] Tzalenchuk A et al 2010 Towards a quantum resistance standard based on epitaxial graphene *Nat. Nanotechnol.* **5** 186–9
- [10] Rigosi A F et al 2019 Graphene devices for tabletop and high-current quantized hall resistance standards *IEEE Trans. Instrum. Meas.* **68** 1870–8
- [11] Ahlers F et al 2014 The emrp project graphohm—towards quantum resistance metrology based on graphene *29th Conf. Precision Electromagnetic Measurements (CPEM 2014)* pp 548–9
- [12] Callegaro L et al 2020 The EMPIR project GIQS: graphene impedance quantum standard *2020th Conf. Precision Electromagnetic Measurements (CPEM) 24–28 August 2020 (IEEE)* (<https://doi.org/10.1109/CPEM49742.2020.9191743>)
- [13] Benz S P and Hamilton C A 1996 A pulse-driven programmable Josephson voltage standard *Appl. Phys. Lett.* **68** 3171–3
- [14] Overney F, Flowers-Jacobs N E, Jeanneret B, Rüfenacht A, Fox A E, Underwood J M, Koffman A D and Benz S P 2016 Josephson-based full digital bridge for high-accuracy impedance comparisons *Metrologia* **53** 1045
- [15] Bauer S, Behr R, Hagen T, Kieler O, Lee J, Palafox L and Schurr J 2017 A novel two-terminal-pair pulse-driven Josephson impedance bridge linking a 10 nF capacitance standard to the quantized hall resistance *Metrologia* **54** 152–60
- [16] Overney F, Flowers-Jacobs N, Jeanneret B, Rüfenacht A, Fox A, Dresselhaus P and Benz S 2020 Dual Josephson impedance bridge: towards a universal bridge for impedance metrology *Metrologia* **57** 065014
- [17] Bauer S, Pimsut Y, Behr R, Kieler O, Kruskopf M, Palafox L, Lee J and Schurr J 2020 AC quantum hall resistance combined with a four-terminal pair pulse-driven Josephson impedance bridge *2020th Conf. Precision Electromagnetic Measurements (CPEM 2020) 24–28 August 2020 (IEEE)* (<https://doi.org/10.1109/CPEM49742.2020.9191895>)

- [18] Benz S P, Burroughs C J and Dresselhaus P D 2001 AC coupling technique for Josephson waveform synthesis *IEEE Trans. Appl. Supercond.* **11** 612–16
- [19] Bauer S, Behr R, Kieler O, Lee J, Palafox L and Schurr J 2018 progress on PTB's pulse-driven Josephson impedance bridge combined with an AC quantum hall resistance *2018th Conf. Precision Electromagnetic Measurements (CPEM 2018)*
- [20] Delahaye F 1993 Series and parallel connection of multiterminal quantum Hall effect devices *J. Appl. Phys.* **73** 7914–20
- [21] Jeanneret B 2001 AC QHR sample holder, final report of Euramet project 540, reg. no. 540 *Tech. rep.* EURAMET (available at: www.euramet.org/technical-committees/tc-projects/)
- [22] Kruskopf M and Elmquist R E 2018 Epitaxial graphene for quantum resistance metrology *Metrologia* **55** R27–R36
- [23] Rigosi A F *et al* 2019 Gateless and reversible Carrier density tunability in epitaxial graphene devices functionalized with chromium tricarbonyl *Carbon* **142** 468–74
- [24] Kruskopf M, Rigosi A F, Panna A R, Patel D K, Jin H, Marzano M, Berilla M, Newell D B and Elmquist R E 2019 Two-terminal and multi-terminal designs for next-generation quantized hall resistance standards: contact material and geometry *IEEE Trans. Electron. Devices* **66** 3973–7
- [25] Kruskopf M *et al* 2020 Graphene quantum hall effect devices for AC and DC resistance metrology *2020th Conf. Precision Electromagnetic Measurements (CPEM 2020)* submitted (IEEE) (<https://doi.org/10.1109/CPEM49742.2020.9191851>)
- [26] Schurr J, Moser H, Pierz K, Ramm G and Kibble B P 2011 Johnson-Nyquist noise of the quantized Hall resistance *IEEE Trans. Instrum. Meas.* **60** 2280–5